The percolation limits for two-phase blends of PMMA and copolymers of styrene and MMA

L. N. Andradi and G. P. Hellmann*
Deutsches Kunststoff-Institut, D-6100 Darmstadt, Germany
(Received 18 July 1990; revised 5 May 1992)

Phase separation and phase structure growth were studied, in the temperature range 150–220°C, in blends of poly(methyl methacrylate) (PMMA) and random copolymers of styrene and methyl methacrylate [$P(S_xMMA_{1-x})$] with $x \geqslant 0.4$. Blends with $0.4 \leqslant x < 0.6$ are homogeneous at lower temperatures. One-phase films of these blends were cast at room temperature from solution. Granules of all blends with $0.4 \leqslant x \leqslant 1$ were made by extrusion at 180°C. They had a fine two-phase morphology. Isothermal structure evolution was studied with both types of blends. The types of morphology and the structure growth rates were investigated, particularly in late stages where growth proceeds under steady-state conditions. The percolation limits between domain–matrix and cocontinuous morphologies were determined as a function of the incompatibility, χ/χ_c, which strongly increases with x in the blend series. The percolation range proved to be similar to the spinodal range at low χ/χ_c, but not at high χ/χ_c, where cocontinuous morphologies are found in a narrow range only.

(Keywords: thermoplastic polymer blends; phase morphologies; percolation limits; compatibility)

INTRODUCTION

Phase separation and phase structure growth can be studied well in thermoplastic blends[1–3]. In the highly viscous matrices, all processes are conveniently slow. Intermediate morphologies can be frozen in. Blends where both components are thermoplastics with similar viscosities in the liquid state are particularly suited. A well known study was published by McMaster on the morphologies of a blend of poly(methyl methacrylate) (PMMA) and a random copolymer of styrene and acrylonitrile[1]. Some parts of the study discussed below are similar.

The phase structures of blends of PMMA and random copolymers of styrene and MMA [$P(S_xMMA_{1-x})$], referred to as PMMA/x, including polystyrene (PS) itself, were analysed. Isothermal phase structure growth was monitored in two kinds of blends: (1) homogeneous blends where phase separation had been induced by temperature jumps; and (2) two-phase blends that had been dispersed as finely as possible by extrusion.

Various theories[4–15], notably those by Cahn[5–7], Furukawa[14], and Siggia[15], describe phase separation in its different stages. Our interest focused on the 'late stages', where the three types of morphology shown in *Figure 1*, M_A, M_B, and CC, are formed. Which of them is observed in a blend A/B depends on the phase volume:

$$\psi = \frac{\phi - \phi''}{\phi' - \phi''} \qquad (1)$$

given by the volume fractions of the component A in the two coexisting phases (ϕ', ϕ'') and in the blend (ϕ). ψ is the volume fraction of the phase richer in A ($\phi' > \phi''$).

At low ψ, spherical domains of A are embedded in a matrix of B (type M_B) while the roles are reversed at high ψ (type M_A). In between, cocontinuous structures of two interpenetrating phase networks are formed (type CC). The coarseness r of the morphologies is given by the diameter of the spheres or the thickness of the network strands. Since the interface between phase domains is unstable, r grows in time.

The question arises as to whether, during structure growth, the types of morphology change, too. Many properties, particularly the permeability, would respond strongly should there be transitions $M_A \rightarrow CC$ or $M_B \rightarrow CC$. Drastic effects are known in colloids where the conductivity responds[16]. Transitions $M_A \rightarrow CC$ and $M_B \rightarrow CC$ are *percolation* transitions where the formerly disperse minor phase becomes continuous. The percolation limits were studied.

THEORY

The different stages of phase separation are briefly characterized, to define the late stages that were studied. Phase separation of a blend A/B starts in the homogeneous state and ends in an equilibrium state of a bilayer with one phase floating on top of the other (denser) phase. Structure growth kinetics are expected to change twice.

- In the early stages, the dynamics are not basically different from those in the homogeneous state. Structure fluctuations are driven by chain diffusion, except that now permanent concentration modulations are created[5–10,17–19].

* To whom correspondence should be addressed

0032-3861/93/050925-08

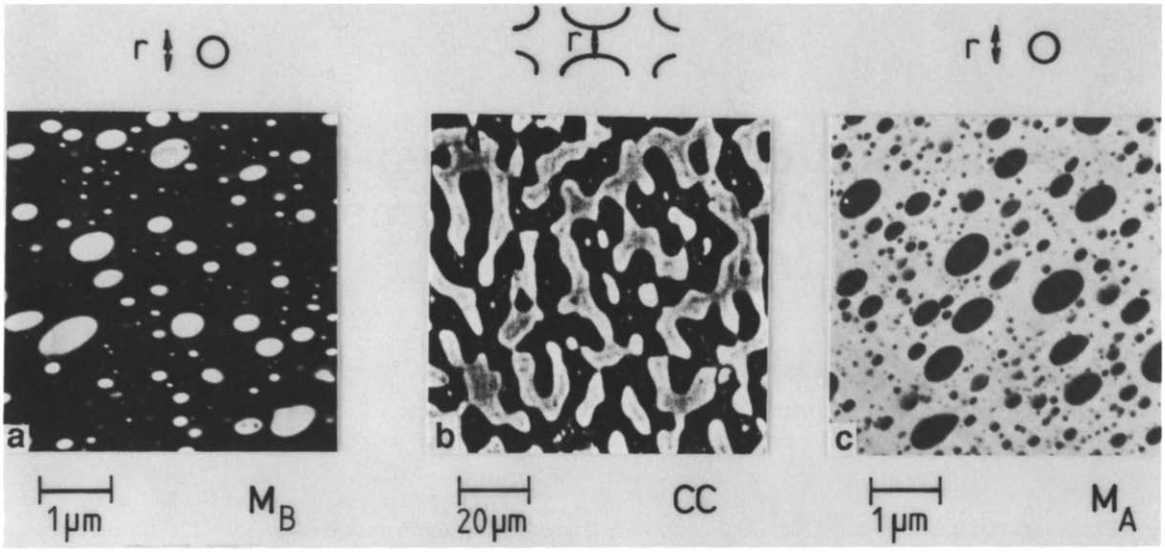

Figure 1 Light micrographs of blends PMMA/PS in late stages of phase structure growth. ψ = (a) 0.25, (b) 0.50, (c) 0.75; r = coarseness parameter

- In the late stages, the coexisting phases have the equilibrium compositions ϕ' and ϕ''. The structure is no longer changed by chain diffusion, but by motions of and in phase domains[1,14,15].
- In the final stages, the coarseness of structure exceeds at least one of the sample dimensions. Such coarse morphologies keep growing in less than three dimensions. The rates and structures change considerably, until the equilibrium state of a bilayer is eventually established[20,21].

Only the early and late stages are considered in this paper, the final stages will be discussed in a forthcoming paper.

The Flory–Huggins model[22] yields a prediction of the early stages of phase separation. A blend A/B of polymers of equal chain volumes $V_A = V_B = \bar{V}$ exhibits a critical point at:

$$\chi = \chi_c = 2/\bar{V} \tag{2}$$

and, if $\chi > \chi_c$, a symmetric miscibility gap $\Delta\phi = (\phi' - \phi'')$ given by

$$\frac{1}{\Delta\phi} \ln \frac{1 + \Delta\phi}{1 - \Delta\phi} = 2\chi/\chi_c \tag{3}$$

and a spinodal range $\Delta\phi_s = (\phi_s' - \phi_s'')$ given by

$$\Delta\phi_s^2 = 1 - \chi_c/\chi \tag{4}$$

Both are shown in *Figure 2*, as functions of the 'incompatibility χ/χ_c' of the blend components. Later, in the blend series PMMA/x, the incompatibility will be varied strongly. It is connected, by $\sigma \approx \sqrt{\chi/\chi_c - 1}$, to the driving force of structure growth[23], the interfacial tension σ.

A homogeneous blend is unstable within $\Delta\phi_s$, and it is metastable outside $\Delta\phi_s$ (still inside $\Delta\phi$). The spinodals are, therefore, expected to separate two regimes of different phase separation kinetics. A regular pattern of periodic concentration modulations should develop inside $\Delta\phi_s$, by the mechanism of spinodal segregation, while an irregular pattern of separate phase domains should develop outside $\Delta\phi_s$, by a thermally activated mechanism.

It is tempting to assume that morphologies inside $\Delta\phi_s$ are always of type CC (*Figure 1b*), and outside $\Delta\phi_s$, always of type M_A or M_B (*Figure 1a, c*). However, that

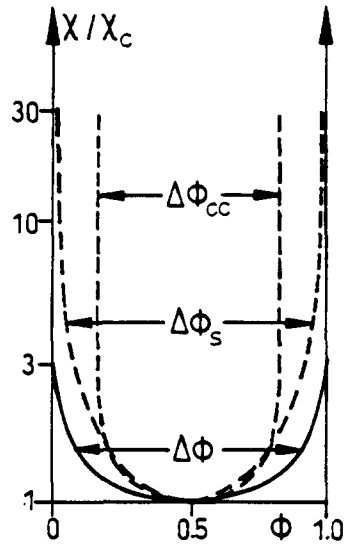

Figure 2 Universal phase diagram with the incompatibility χ/χ_c in the ordinate. $\Delta\phi$ = miscibility gap (equation (3)); $\Delta\phi_s$ = spinodal range (equation (4)); $\Delta\phi_{CC}$ = percolation range (equation (5))

cannot be true, since blends with high χ/χ_c would exhibit exclusively CC morphologies ($\Delta\phi_s \cong \Delta\phi \cong 1$, *Figure 2*). On closer inspection, spinodals are not well defined limits. There is a gradual rather than a sharp transition from the metastable to the unstable regime[24]. Further, the concept of spinodals is limited to the first stages of phase separation, where the linear assumptions for chain diffusion dynamics hold. These assumptions become invalid when segregation produces two well defined phases with the composition ϕ' and ϕ''.

The components in the late stages are no longer in contact, except at the interfaces, and structure growth is no longer driven by chain diffusion. The structures grow rather due to processes as indicated in *Figure 3*. Only the lower half of the phase volume axis of a two-phase blend A/B is considered ($0 < \psi < 1/2$). Spheres of A in a matrix of B (type M_B) are observed at lower ψ and a cocontinuous phase network (type CC) at higher ψ. The spheres on the left coalesce to deformed domains (τ_1), whereupon either the spherical shape is restored (τ_2), or further spheres are added (τ_1). Strands that are formed in the latter process can break up again (τ_{-1}), due to

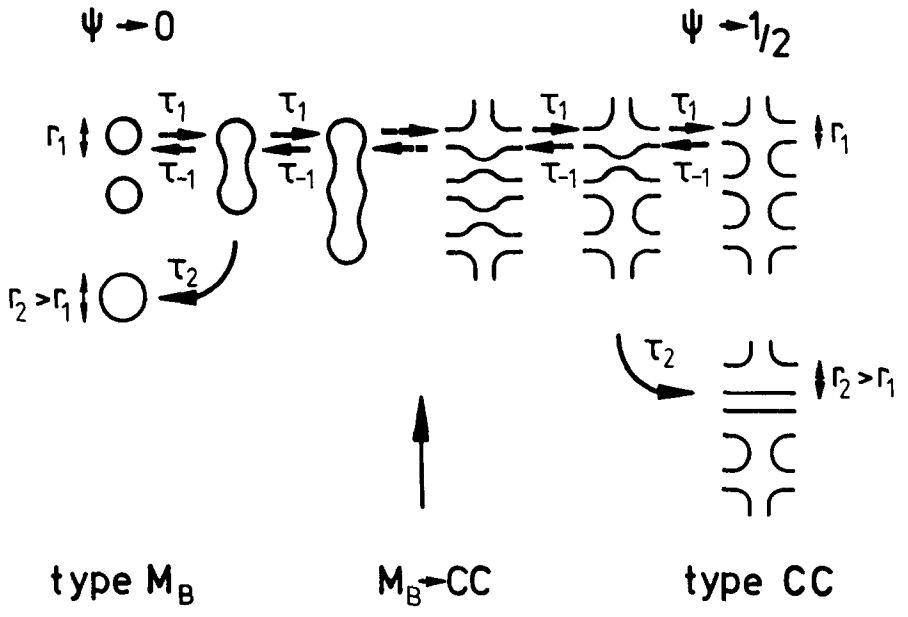

Figure 3 Scheme of phase structure growth in the range $0 < \psi < 1/2$ of phase volumes (see text). τ_i = time constants; r_i = coarseness parameters

Table 1 Homopolymers and copolymers of styrene and MMA

	x	$10^{-3} \times M_w$	M_w/M_n	V_w (nm^3)	χ/χ_c (180°C)	T_g (°C)
PMMA	0	94	2.1	132	0	122
$P(S_xMMA_{1-x})$	0.4	81	2.3	120	0.83 (1.1)	112
	0.5	76	2.3	114	2.0	110
	0.6	84	2.3	127	4.2	108
	0.8	107	3.4	165	13	106
PS	1	78	1.7	126	32	105
				$\bar{V} = 131$		

unstable intensification of thickness fluctuations[25]. Similar processes take place on the right of *Figure 3*, in the phase network. The percolation limit $M_B \rightarrow CC$ is somewhere in the centre of *Figure 3*.

Of the time parameters, τ_1 depends on the phase volume ψ, τ_2 on the incompatibility χ/χ_c, and τ_{-1} depends on both. Process 2 leads to coarsening. The processes 1 and -1 establish, in the steady state, an equilibrium. At the percolation limit, both are equally effective.

The percolation limits $M_A \rightarrow CC$ and $M_B \rightarrow CC$ have so far not been studied intensively. Random percolation is expected when, in a hexagonally dense packing of two types of spheres (i.e. phase domains), at least two of the 12 neighbours of a given sphere are of its own type. That happens inside the percolation range $\Delta\psi_{CC} = (\psi'_{CC} - \psi''_{CC})$ with $\psi'_{CC} = 5/6$ and $\psi''_{CC} = 1/6$, so that

$$\Delta\psi_{CC} = \Delta\phi_{CC}/\Delta\phi = 0.67 \quad (5)$$

CC structures should appear inside $\Delta\psi_{CC}$, and M_A or M_B structures outside $\Delta\psi_{CC}$. The percolation range in terms of blend compositions, $\Delta\phi_{CC} = (\phi'_{CC} - \phi''_{CC})$, is shown in *Figure 2*. Note that $\Delta\psi_{CC}$ is assumed to be independent of χ/χ_c and of the structure coarseness r. This is checked below.

The position of the percolation limits is important since structure growth is predicted to be very different for the types M_A, M_B and CC. For types M_A and M_B, structures should coarsen as[4,26,27]

$$r \approx t^{1/3} \quad (6)$$

Efforts to model the more complex growth of CC types, from the early through some intermediate to the late stages, are still in progress[4–15]. Coarseness should increase with a stage-dependent exponent, the final law in the late stages being[14,15]

$$r \approx t \quad (7)$$

In these stages, CC structures are expected to grow self-similarly, under steady-state conditions[14,15,17–19].

EXPERIMENTAL

The polymers PMMA, PS, and $P(S_xMMA_{1-x})$, synthesized by radical polymerization, were obtained from Röhm AG. Some data are listed in *Table 1*. Copolymer compositions x were measured by elemental analysis and ^1H n.m.r. spectroscopy (x is the volume fraction of styrene, as called for by the Flory–Huggins model). Molecular weight data were obtained by g.p.c., with the calibration scales of PMMA and PS averaged. The volume per chain is given by $V_w = M_w/\rho N_A$, where ρ is the density and N_A the Avogadro number. V_w is always similar, only the (less important) copolymer $x = 0.8$ is far from the average $\bar{V}$, which was used to calculate the critical interaction parameter χ_c

(equation (2)). The interaction parameter χ of the blends PMMA/x had been determined in ref. 28 from the miscibility windows of blends $P(S_xMMA_{1-x})/P(S_yMMA_{1-y})$. The interaction parameters of these blends were given approximately by

$$\chi_{xy} = (x^2 - y^2)^2 \chi_{S-MMA}$$

For $y = 0$, *i.e.* for the blends PMMA/x of *Table 1*, this yields:

$$\chi = x^4 \chi_{S-MMA}, \qquad \chi_{S-MMA}(180°C) = 0.5\ nm^{-3} \quad (8)$$

where χ_{S-MMA} is the interaction parameter of the homopolymer blend PMMA/PS[28]. The incompatibility χ/χ_c in *Table 1* was calculated with equations (2) and (8). Glass transition temperatures, T_g, were determined by d.s.c. at a heating rate of 20 K min^{-1}.

Phase diagrams of the blends PMMA/x were determined using a film casting technique discussed elsewhere, with toluene as the solvent. These phase diagrams show the miscibility of blends even below T_g.

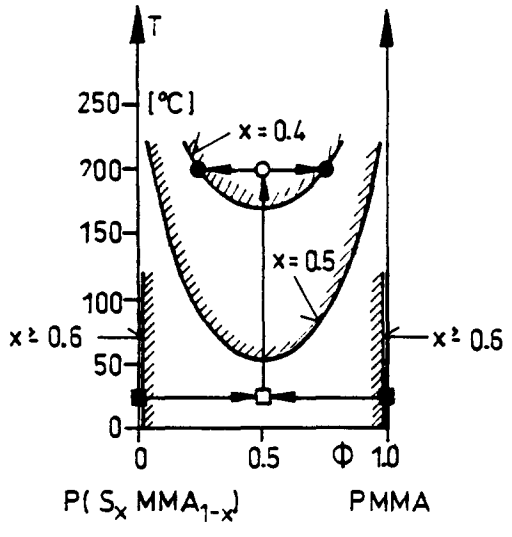

Figure 4 Phase diagrams of blends PMMA/x, determined using cast films

The blends PMMA/$x = 0.4$ and PMMA/$x = 0.5$ have high-temperature miscibility gaps as shown in Figure 4. The critical temperature $T_{cx=0.4} = 170°C$ is at odds with $\chi/\chi_c < 1$ in *Table 1* which must be replaced, as indicated, by $\chi/\chi_c \cong 1.1$. (Equation (8) is an approximation.) This correction will not alter the conclusions.

Homogeneous films ($\cong 200\ \mu m$ thick) of the blends PMMA/$x = 0.4$ and PMMA/$x = 0.5$ were prepared by film casting from toluene solution at room temperature. The films were dried at 100°C (i.e. below T_g) for 7 days, then they were heated rapidly to a temperature in the miscibility gap and demixed isothermally. The sequence of processes is indicated in *Figure 4*.

Two-phase granules (2 mm thick) of all blends PMMA/x were prepared by triple extrusion at 190°C in a single screw extruder (Brabender, $L/D = 20$, $D = 19$ mm) at 60 rev min^{-1} and subsequent cooling in air. After three extrusion cycles, the phase structures did not change anymore.

After temperature jumps from room temperature, films and granules were annealed for different times at constant temperature in tightly fitting holders in an aluminium block oven, and then quenched. Thin sections were cut from the centre of the samples, normal to the film plane or perpendicular to the extrusion direction in the granules, with an ultramicrotome, for inspection by interference contrast light miscroscopy (LM Metalloplan, Leitz) or transmission electron microscopy (TEM, Elmiskop 1a, Siemens). Etching was unnecessary to obtain contrast, because the refractive indices and the stability in the electron beam of the blend components were sufficiently different. Sections were 1 μm thick for LM and 50 nm for TEM.

RESULTS

Isothermal phase separation in initially homogeneous blends and isothermal phase structure growth in initially two-phase blends were studied microscopically up to a structure coarseness one-quarter of the smallest sample dimension. The temperature was varied in the interval 150–220°C, i.e. approximately 40–110°C above T_g.

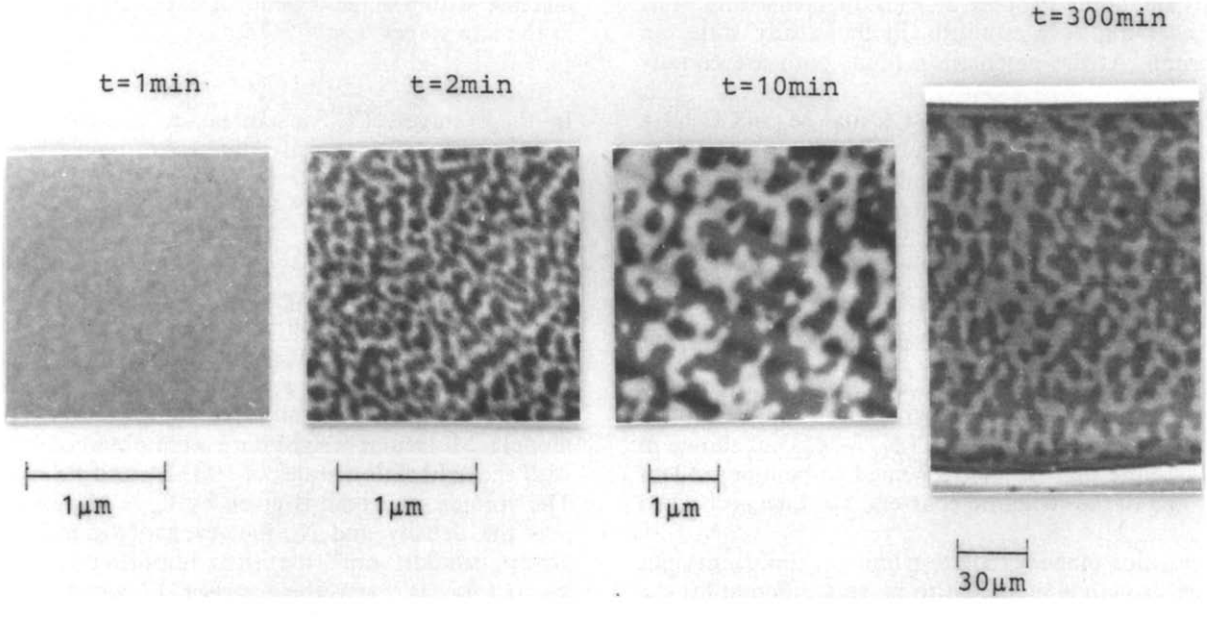

Figure 5 Electron and light micrographs of the blend PMMA/$x = 0.5$ with $\phi = 0.50$, taken during phase separation at 190°C

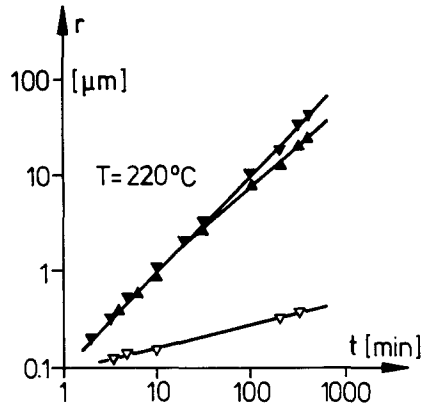

Figure 6 Coarseness r of phase structures in blends PMMA/x = 0.5 at 220°C with ϕ = ▼, 0.50 (lamellar CC); ▲, 0.25 (cylindric CC); ▽, 0.20 (M_B structure)

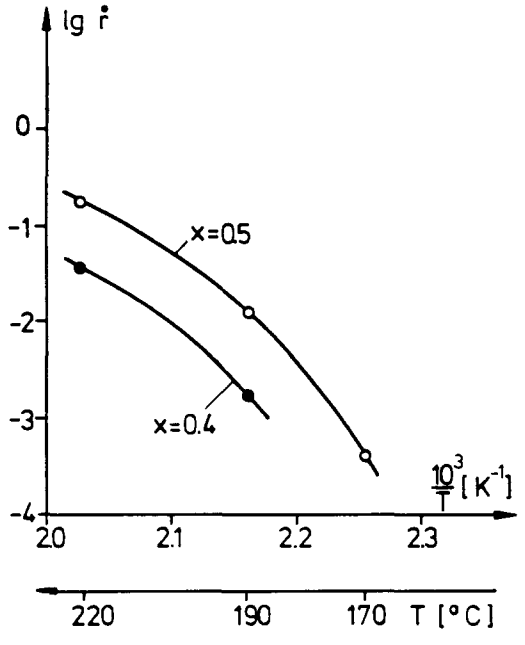

Figure 7 Arrhenius diagram of the structure growth rate $\dot{r}$ of blends PMMA/x with ϕ = 0.50

Phase separation in initially homogeneous blends

Homogeneous films of the blends PMMA/x = 0.4 and PMMA/x = 0.5 with different compositions ϕ were demixed isothermally inside the miscibility gap (*Figure 4*).

Figure 5 shows morphologies of the blend PMMA/x = 0.5 (ϕ = 0.50) that were formed during phase separation at 190°C. Contrast is poor in the first picture, where the structure coarseness is still on the order of the thickness of the TEM section. The last picture shows a perpendicular section through the entire film layer. The phase structures are of type CC throughout. Similar pictures were obtained at the other temperatures.

Clearly, the only parameter changing is the coarseness r which was determined by averaging over the thickness of the network strands (in large pictures). Linear growth, as shown in *Figure 6* (ϕ = 0.50), was observed at all times and temperatures, which agrees with equation (7).

More specifically, theory predicts $r \approx (\sigma/\eta)t$ for cocontinuous morphologies[15], where σ is the interfacial tension and η is the matrix viscosity (for ϕ = 0.50 the average viscosity). The temperature dependence of the growth rate $\dot{r}$ is shown in *Figure 7*. There is also a curve in *Figure 7* for the blend PMMA/x = 0.4 (ϕ = 0.50). Both curves follow a Williams–Landel–Ferry (WLF) law that describes primarily the temperature behaviour of the viscosity η. The blends PMMA/x = 0.4 and PMMA/x = 0.5 behave differently due to different interfacial tensions $\sigma \approx \sqrt{\chi/\chi_c - 1}$ (*Table 1*).

The cocontinuous morphologies in *Figure 5* are clearly self-similar, and the growth law in *Figure 6* (ϕ = 0.50) is linear. While a rigorous test of the structure factors (as is possible with light scattering[17–19]) cannot be made on the basis of microscopic pictures, *Figures 5* and *6* leave no doubt that the CC structures grow under steady-state

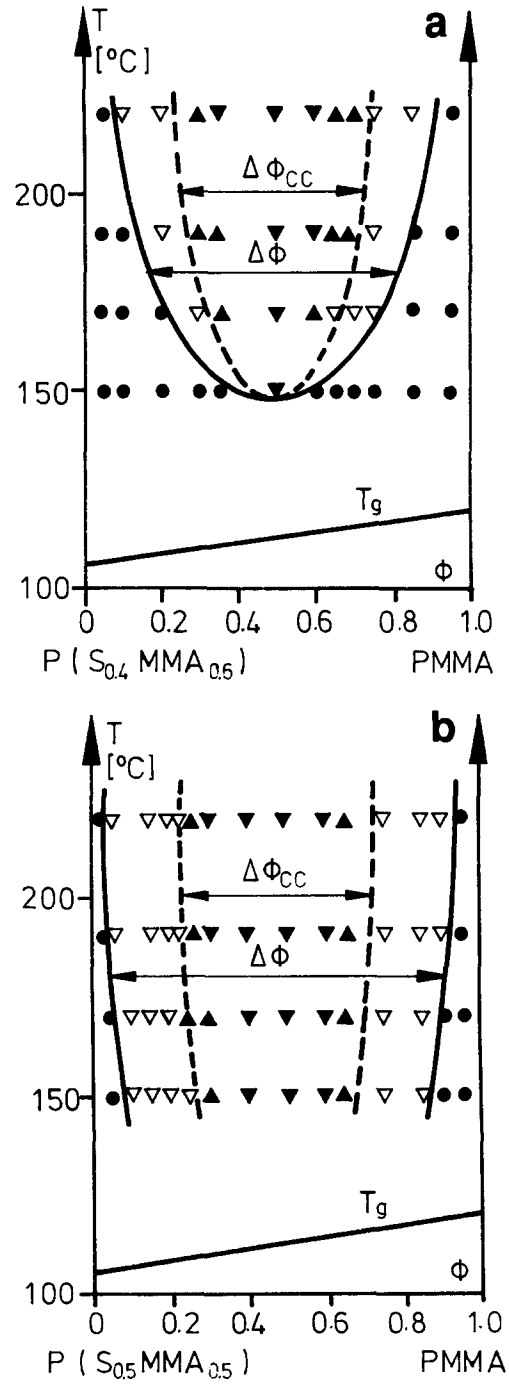

Figure 8 Phase diagrams of blends PMMA/x with (a) x = 0.4 and (b) x = 0.5, deduced from TEM observations. $\Delta\phi_{cc}$ = percolation range. ▽, M_A or M_B; ▲, cylindric CC; ▼, lamellar CC structures; ●, homogeneous

conditions, from the moment where they become visible in TEM.

The phase diagrams of *Figure 8* show the distribution of structure types for the blends PMMA/$x = 0.4$ and PMMA/$x = 0.5$. The miscibility gaps are close to those of *Figure 4*. Type CC structures are found in the centre, type M_A and M_B structures at the sides of the gaps.

In M_A and M_B morphologies, the coarseness was determined by averaging over the diameters of the spheres. The size distribution is broader than in CC structures. Domain growth was found to be given by $r \approx t^{1/4}$ (*Figure 6*, $\phi = 0.20$) which is similar to the prediction of equation (6). *Figure 9* demonstrates that morphologies of type CC grow much faster than those of types M_A and M_B.

All morphologies had the similar attribute that the type never changed while the structure grew considerably, sometimes by 10^3 (50 nm–50 μm). That raised the question of which type would appear at the percolation limits $M_A \rightarrow CC$ and $M_B \rightarrow CC$ and whether it would change in time or not.

When $\phi \leqslant 0.22$ (or $\phi \geqslant 0.75$), the blend PMMA/$x = 0.5$ yields, at 190°C, morphologies with perfect spheres of PMMA (or of PS). *Figure 10* shows the structures for the composition $\phi = 0.25$. The pictures feature PMMA domains of an irregular shape that seem to attempt to connect to a continuous network. Since $\phi = 0.22$ yielded spheres of PMMA in a M_B structure, a transition to type M_B during structure growth might have been expected for $\phi = 0.25$. Yet even the peculiar morphology of *Figure 10 does not change its type* while coarsening by 10^3. Structure growth obviously proceeds again self-similarly under steady-state conditions.

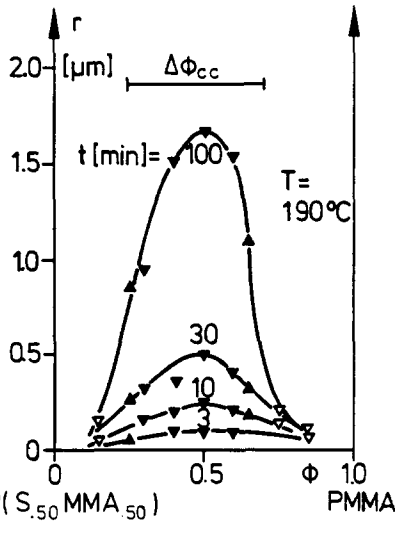

Figure 9 Coarseness r after annealing times t at 190°C in blends PMMA/$x = 0.5$. $\Delta\phi_{CC}$ = percolation range (symbols as in *Figure 8*)

Analysis of a series of consecutive TEM sections cut at the same spot from the blend PMMA/$x = 0.5$ ($\phi = 0.25$) of *Figure 10*, and from similar blends, revealed that the minor phase in fact forms, in three dimensions, a truly continuous network. The discontinuous domains seen in each single, two-dimensional TEM section are parts of an unordered three-dimensional network of approximately cylindrical strands. *Figure 10* thus shows CC morphologies. The difference to the CC structures of *Figure 5*, which look cocontinuous even in TEM sections, is that the latter form, in three dimensions, an unordered *lamellar* phase network. As can be seen in *Figure 6*, the CC structures of *Figure 1* and *Figure 10* grow at similar rates.

The percolation limits are positioned between the cylindrical CC morphologies of *Figure 10* and the disperse M_A or M_B morphologies of *Figures 1a*, and *c*, as shown in *Figure 8*. These percolation limits mark sharp, not gradual transitions.

Figure 8 yields percolation ranges of $\Delta\psi_{CC} = 0.61$ for PMMA/$x = 0.4$ and $\Delta\psi_{CC} = 0.55$ for PMMA/$x = 0.5$. This is not too far from equation (5). Note that the percolation limits are constant. *Figure 8* describes extremely fine as well as very coarse structures.

Structure growth in initially two-phase blends

Since the initially homogeneous blends had been, in all detectable stages, in a steady state, an attempt was made to produce this state with immiscible blends.

First, the blends PMMA/$x = 0.4$ and PMMA/$x = 0.5$ were prepared by extrusion in the miscibility gap. Immediately after extrusion, the samples had morphologies of the low coarseness $r \leqslant 0.2$ μm. Their structure

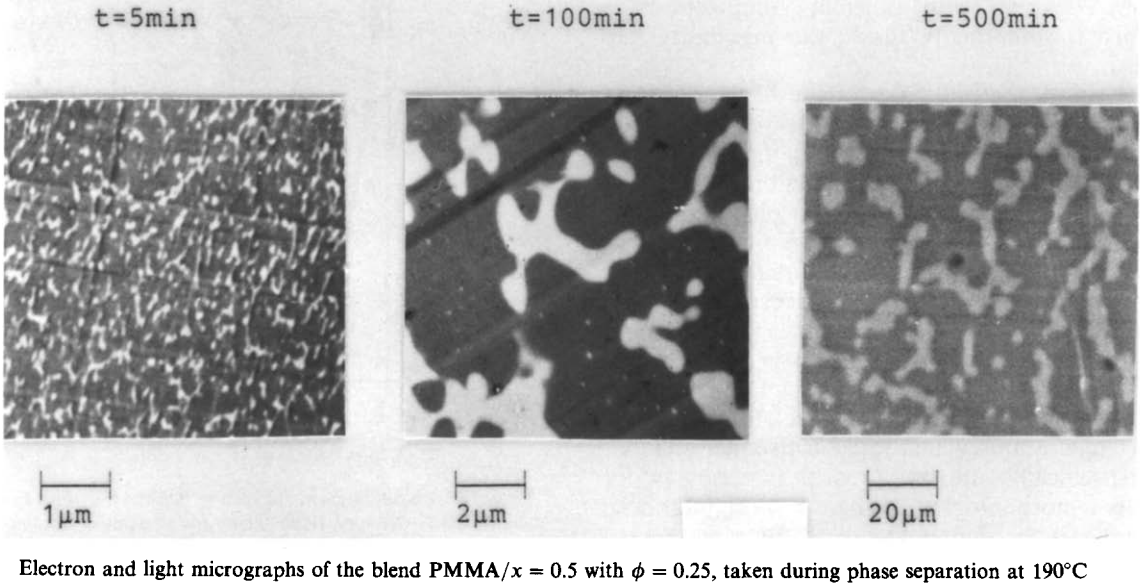

Figure 10 Electron and light micrographs of the blend PMMA/$x = 0.5$ with $\phi = 0.25$, taken during phase separation at 190°C

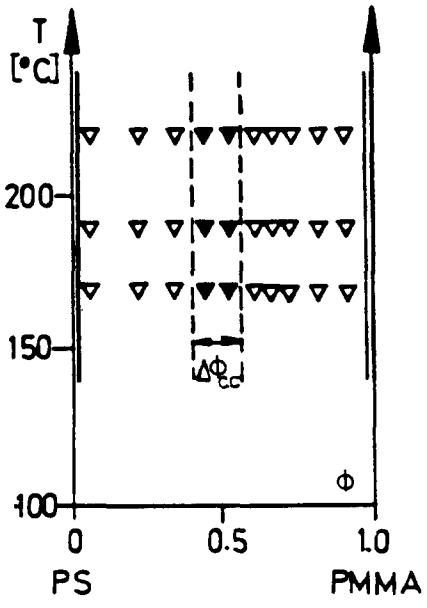

Figure 11 Phase diagram of the blend PMMA/PS, deduced from TEM observations. $\Delta\phi_{CC}$ = percolation range. ▽, M_A or M_B; ▼, lamellar CC structures

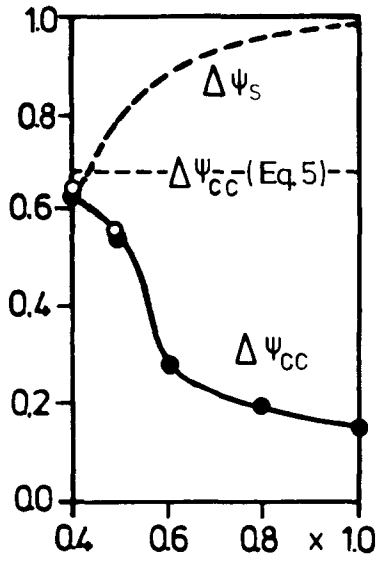

Figure 12 Percolation range $\Delta\psi_{CC}$, given by equation (5) and determined from initially one-phase (○) and initially two-phase (●) blends, and spinodal range $\Delta\psi_s$ of blends PMMA/x

patterns were perturbed by the mechanical force fields. (These patterns will be discussed in a forthcoming paper.) However, upon annealing above T_g, these blends developed, always below $r = 2\ \mu m$, exactly the distribution of structure types shown in *Figure 8*, as had to be expected for steady-state growth.

Similar experiments were then made with the blends PMMA/$x \geqslant 0.6$, which are demixed at all temperatures. The coarseness immediately after extrusion was $r \leqslant 0.5\ \mu m$.

During annealing, the steady state was established, always below $r = 5\ \mu m$.

The miscibility gaps of the blends PMMA/$x \geqslant 0.6$ cover the entire phase diagram ($\Delta\phi \cong 1$). Symmetric percolation ranges were found in their centres, with a width independent of temperature. The phase diagram of the blend PMMA/PS is shown in *Figure 11*. The percolation range is quite narrow. There were no cylindrical CC structures. The morphologies switched directly from M_A or M_B to the lamellar CC type. *Figure 12* shows how the percolation range $\Delta\psi_{CC}$ narrows with increasing x. The blend PMMA/$x = 0.4$, which is close to miscibility, prefers type CC while the blend PMMA/PS, which has the least compatible components, prefers the types M_A and M_B.

Also indicated in *Figure 12* are the predictions for $\Delta\psi_{CC}$ of equation (5) and the width $\Delta\psi_s = \Delta\phi_s/\Delta\phi$ of the spinodal range (*Figure 2*). In contrast to $\Delta\psi_{CC}$, $\Delta\psi_s$ widens with increasing x. It is obvious that $\Delta\psi_s$ has nothing to do with the percolation range.

DISCUSSION

The phase diagrams of *Figure 8* suggest a subdivision of the structure type CC into a lamellar type CL (*Figure 5*) and two cylindrical types, CC_A and CC_B (*Figure 10*). Together with M_A and M_B, there are thus five structure types instead of the three in *Figure 1*. The structural units are spheres, cylinders and lamellae. If these units are ordered in a cubic lattice, the ratios of interface and volume are, for phase volumes $0 < \psi < 1/2$ (exchange $\psi \to 1 - \psi$ for $1/2 < \psi < 1$):

$$I_S = (36\pi\psi)^{2/3} \qquad I_C = (4\pi\psi)^{1/2} \qquad I_L = 2 \qquad (9)$$

There are transition concentrations where $I_S = I_C$ and $I_C = I_L$. Should the structure of the lowest specific interface I always be the stable one, one should observe structures: of the lamellar type CL inside $\Delta\psi_{CL} = 0.36$; and of the cylindrical types CC_A and CC_B outside $\Delta\psi_{CL}$, but still inside $\Delta\psi_{CC} = 0.67$ (which is equal to equation (5)).

The universal miscibility gap of *Figure 2* is repeated in *Figure 13*. The regimes calculated for the cylindric

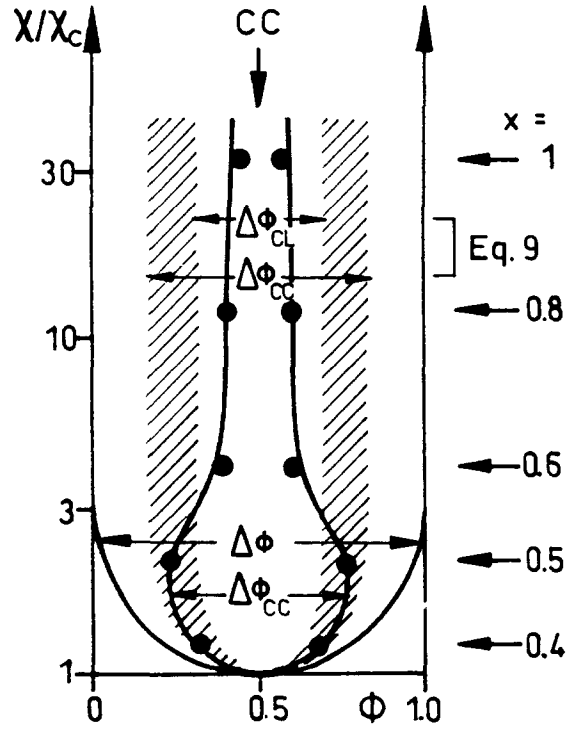

Figure 13 Universal phase diagram (compare with *Figure 2*). The drawn lines (—●—) are the percolation limits determined for blends PMMA/x (*Figure 12*, χ/χ_c from equations (2) and (8)). The shaded areas mark the calculated regions (equation (9)) for CL structures

structures CC_A and CC_B are shaded. Also shown are the measured percolation ranges of *Figure 12*, translated into $\Delta\phi_{CC}$, at the levels of $\chi/\chi_c(x)$ given in *Table 1*. The figure holds for 180°C (equation (8)), but it describes all other temperatures (150–220°C) equally well. $\Delta\psi_{CC}$ never depends on temperature, $\chi/\chi_c(T)$ being a weak function[28]. In contrast, $\chi/\chi_c(x)$ varies strongly from $\chi/\chi_c \cong 1$ to $\chi/\chi_c > 30$ in the blend series PMMA/x. There is probably no single blend existing with such a wide range of χ/χ_c.

The percolation range $\Delta\phi_{CC}$ in *Figure 13* coincides at low χ/χ_c with the prediction of equation (5), and it also coincides with the spinodal range $\Delta\phi_s$ (*Figure 2*). Theory predicts that the structure type should not change during growth, which was indeed observed. At higher χ/χ_c, however, $\Delta\phi_{CC}$ narrows, excluding the regimes of the types CC_A and CC_B, which indeed were no longer observed.

These are the main results. The distribution of types M_A, M_B, and CC is at low incompatibility that of random percolation, but high incompatibility stabilizes the morphologies M_A and M_B. In terms of *Figure 3*, the reason is an acceleration of the process -1 of break-up of network strands. In terms of percolation theory, the effect is due to attractive correlations within clusters which have the same effect as an interfacial tension.

In industry, morphologies that do not coarsen rapidly in the liquid state are often preferred. This points towards the disperse structures M_A and M_B. Inasmuch as these are more frequent in blends with high χ/χ_c, the use of blends of highly incompatible polymers may not always be disadvantageous.

ACKNOWLEDGEMENTS

The authors gratefully acknowledge financial support by the Bundesminister für Forschung und Technologie (BMFT).

REFERENCES

1 McMaster, L. P. *Adv. Chem. Ser.* 1975, **142**, 43
2 Nishi, T., Wang, T. T. and Kwei, T. K. *Macromolecules* 1975, **8**, 227
3 Voigt-Martin, I. G., Leister, K. H., Rosenau, R. and Koningsveld, R. *J. Polym. Sci., Polym. Phys. Edn* 1986, **24**, 723
4 Gunton, J. D., SanMiguel, M. and Sahni, P. S. 'The Dynamics of First-Order Transitions and Critical Phenomena' (Eds C. Domb and J. L. Lebowitz), Academic Press, New York, 1983, vol. 8, p. 267
5 Cahn, J. W. *Acta Metall.* 1961, **9**, 795
6 Cahn, J. W. *J. Chem. Phys.* 1965, **42**, 93
7 Cahn, J. W. *Trans. Metall. Soc. AIME* 1968, **242**, 166
8 DeGennes, P. G. *J. Chem. Phys.* 1980, **72**, 4756
9 Binder, K. *J. Chem. Phys.* 1983, **79**, 6387
10 Strobl, G. R. *Macromolecules* 1985, **18**, 558
11 Langer, J. S., Bar-On, M. and Miller, H. D. *Phys. Rev.* 1975, **A11**, 1417
12 Binder, K. and Stauffer, D. *Phys. Rev. Lett.* 1974, **33**, 1006
13 Kawasaki, K. and Ohta, T. *Progr. Theor. Phys.* 1978, **59**, 362
14 Furukawa, H. *Adv. Phys.* 1985, **34**, 703
15 Siggia, E. *Phys. Rev.* 1979, **A20**, 595
16 Borkovec, M., Eicke, H. F., Hammerich, H. and DasGupta, B. *J. Phys. Chem.* 1988, **92**, 206
17 Hashimoto, T., Itakura, M. and Hasegawa, H. *J. Chem. Phys.* 1986, **85**, 611
18 Hashimoto, T., Itakura, M. and Shimidzu, N. *J. Chem. Phys.* 1986, **85**, 677
19 Kyu, T. and Saldanha, J. M. *J. Polym. Sci., Polym. Phys. Edn* 1990, **28**, 97
20 Reich, S. and Cohen, Y. *J. Polym. Sci., Polym. Phys. Edn* 1981, **19**, 1255
21 Reich, S. *Phys. Lett.* 1986, **114A**, 90
22 Flory, P. J. 'Principles of Polymer Chemistry', Cornell University Press, Ithaca, 1953
23 Helfand, E. *J. Chem. Phys.* 1975, **63**, 2192
24 Binder, K. *Colloid Polym. Sci.* 1987, **265**, 273
25 Tomotika, S. *Proc. R. Soc. London* 1935, **150**, 322
26 Binder, K. and Stauffer, D. *Phys. Rev. Lett.* 1974, **33**, 1006
27 Binder, K. and Stauffer, D. *Adv. Phys.* 1976, **25**, 343
28 Braun, D., Yu, D., Kohl, P. R., Gao, X., Andradi, L. N., Manger, E. and Hellmann, G. P. *J. Polym. Sci., Polym. Phys. Edn* 1992, **30**, 577